American Mineralogist, Volume 59, pages 127–138, 1974

Sector-Zoned Titanaugites: Morphology, Crystal Chemistry, and Growth

IRENE S. LEUNG

Herbert H. Lehman College of the City University of New York, Bronx, New York 10468

Abstract

Chemical zoning in several titanaugites in alkali-rich rocks occurs from core to rim and in distinct sectors. The {100}, {110}, and {010} sectors are enriched in Al, Ti, and Fe, while the {11$\bar{1}$} sectors are enriched in Si and Mg. Observed geometric configurations of sectors and hourglass structures can be related to a 12-pyramid morphological model.

The growth of clinopyroxenes is discussed in reference to the crystal structure and the distribution of *M* sites in particular. A model is presented using constitutional supercooling and diffusion mechanisms in an attempt to explain sectoral fractionation of the elements during rapid disequilibrium crystallization.

Introduction

Sectoral growth has been observed in a variety of minerals and is clearly related to the conditions of growth, internal and external to the crystal. As early as 1896, Pelikan (1896) recognized the violet-grey titanaugites commonly occurring in alkali-rich magmas, described with great accuracy their Schichtenbau (layered structure), Anwachskegel (growth cone), Sanduhrstructur (hourglass structure), and pointed out that strong color differences and change in optical properties in different portions of the crystals were due to the presence of impurities. Although he did not elaborate on the geometrical details of the growth sectors, they were accurately delineated in his simple sketches of the crystals. More recent studies on sector zoning include those on galena, calcite (Frondel, Newhouse, and Jarrell, 1942), quartz (Cohen, 1960), chloritoid (Halferdahl, 1961), sphalerite (Barton, Bethke, and Toulmin, 1963), plagioclase (Vance, 1965), augite (Farquhar, 1960; Preston, 1966; Strong, 1969; Smith and Carmichael, 1969; Leung, 1971; Gray, 1971; Hollister and Gancarz, 1971), staurolite (Hollister, 1970), gypsum (Kastner, 1970), idocrase (Arem, 1970), and other minerals such as apatite, fluorite, epidote, barite, brookite, apophyllite, zircon, and garnet.

A remarkable feature of sector-zoned crystals is that the crystal faces present are of low-index forms, and that each form produces sectors having characteristic properties. Ideas of crystal growth based on and developed from the Bravais law of reticular density advocate that the structure of a growing crystal face is the rate-determining factor for the velocity of growth in the direction perpendicular to that crystal face. It is well-known that the slowest-growing faces constitute the dominant forms which, in turn, formulate the crystal habit. Sector zoning or compositional difference between growth sectors is generally insignificant in the major elements, but the minor elements are strongly fractionated.

The present study is concerned with the morphology, substructure, chemical compositions, and growth of some sector-zoned, patchy, discontinuous, or mixed titaniferous augite crystals. A model is proposed in an attempt to illustrate rapid disequilibrium crystallization from a melt. The abundance of sector-zoned clinopyroxenes in the Apollo 11 specimens from the moon stimulated interest in the subject, and it is hoped that a study of terrestrial material might also elucidate problems on the thermal history of lunar pyroxenes.

Materials

Two of the samples used in this study are alkaline olivine basalts provided by Professor Richard Armstrong. The first is a suite of rocks from recent extrusive lava flows from McMurdo, Antarctica; the second is a series of volcanic rocks from Goldfield, Nevada, collected by Professor D. J. Vitaliano. A feldspathoidal jacupirangite was obtained from Professor John Gittins and was collected by Dr. D. H. Watkinson from Hessereau Hill, Oka, Quebec. An

essexite from Crawfordjohn, Scotland, was provided by Professor Thomas Pearce. Thin sections of specimens from Germany (Löbauerberg), France, Italy, Brazil, and the United States have also been studied. All the samples are of a continental origin, contain abundant euhedral augite crystals, and show layered growth and sector zoning.

Observations

Optical

Augite crystals in the specimens are euhedral to subhedral, with many grains showing one to four colorless and light brown, moderately pleochroic sectors. The colored sectors are prism sectors, {100}, {110}, and {010}, in the zone of *c*. Basal sections (Fig. 1A), typically ultra-brown and ultra-blue in interference colors, show light brown trapezoidal sectors (prism sectors) surrounding a pseudo-octagonal colorless core ({11$\bar{1}$} sectors). Crystals not showing distinct geometric patterns are also dichroic in character but with patchy color zones. Without exceptions, the crystals are built of growth layers parallel to the crystal faces. The growth layers are discernible optically as sharp thin bands when tilted to vertical on the universal-stage. When the growth layers lie oblique to the plane of a thin section, they appear quite thick, resembling rhythmic compositional zoning although they cannot always be correlated with changes in composition.

Augite crystals approximately 0.2–5.0 mm in size were studied optically by means of universal-stage techniques. As exsolution lamellae are lacking and cleavages are generally absent, poor, or indistinct, the orientation of the crystals was often determined using growth layers parallel to low-index planes. Boundaries of sectors and hourglass structures correspond to crystallographically irrational planes. The crystals are monoclinic, with $2V$ = 49–67°, and $Z \wedge c$ = 41–53°. Optical properties show considerable variations even within the same crystal. Values of $2V$, for instance, range from 53–67° from core to rim in one crystal, and from 49–54° in the same direction in another, both occurring in a specimen from Goldfield. The *c*-axes of the crystals were, in general, determined from measurements of either the {100}, {110} growth layers or the {110} cleavage. Extinction angles, $Z \wedge c$, are consistently smaller by 4–8° in the {11$\bar{1}$} sector than in the {100} sector, apparently due to chemical variations.

The geometric configuration of sectors constituting the hourglass structure is closely related to the distance of the section from the center of the crystal and to the direction in which the crystal is viewed. Some of the representative types are described below.

Type 1: Sections nearly normal to *c* show trapezoidal sectors around a central core (Fig. 1A). The central core may be quite large, or almost nonexistent, dependent on the distance of the section from the center of the crystal (Figs. 2F and 2G).

Type 2: Two types of structures have been observed in sections nearly normal to *b*: (a) sections showing four triangular sectors whose apices converge at a central point (Fig. 1B, larger crystal, corresponding to Fig. 2A), and (b) sections showing only two triangular sectors which do not meet at a point (Fig. 1B, smaller crystal, corresponding to Fig. 2D). The former represents a section passing through the center of the crystal, whereas the latter is cut some distance from the center.

Type 3: Sections oblique to *b* showing only one triangular sector (Fig. 1C, corresponding to Fig. 2E).

Type 4: Sections nearly normal to *a* or one of the optic axes may show sectors of the types shown in Figure 1B, but the interference colors will be of the first order gray for a section of standard thickness.

The prism sectors are pleochroic (light brown), and all the following forms are of common occurrence: {100}, {110}, and {010}. The non-prism, colorless sectors are of the form {11$\bar{1}$}. No higher-index forms have so far been observed apart from possible unidentified sectors which lack good morphological features. The optical indicatrices of different sectors differ in orientation by a few degrees to about 10 degrees.

X-Ray

Well-defined growth sectors of augite crystals from Goldfield and McMurdo were identified optically, then portions of individual sectors were separated from thin sections and mounted as single crystals for X-ray diffraction studies. Pyroxenes from both localities have the diopside structure (space group $C2/c$) and contain no exsolved phases. Reflections on precession photographs are sharp, but Laue photographs of the same crystal fragments show moderate asterism or stretching of the X-ray spots. More intense X-ray asterism is generally observed in the {100} than in the {11$\bar{1}$} sectors. A single crystal consisting, optically, of equal portions of a (100) and a (11$\bar{1}$) sector showed tripling of all reflections on the $h0l$ reciprocal lattice net, indicating the

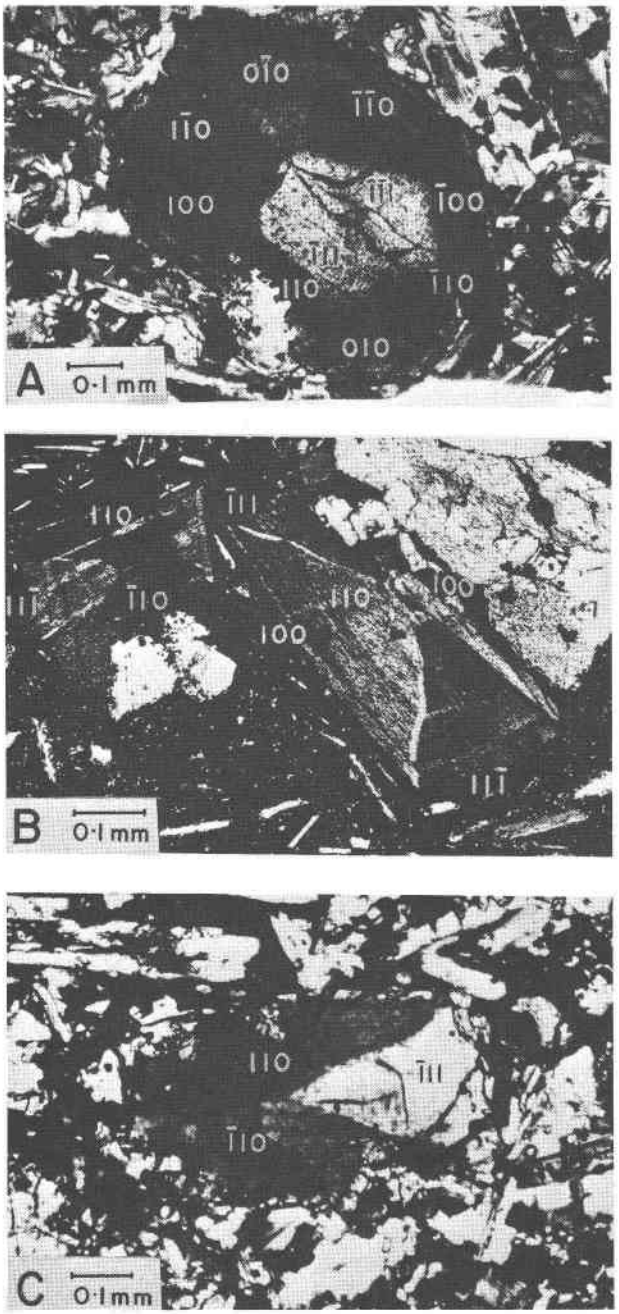

FIG. 1. Photomicrographs of sector-zoned titanaugites, between crossed polarizers. A. Basal section, almost perpendicular to the *c*-axis. Section corresponds to Figures 2G and 3D. Specimen from Goldfield, Nevada. B. Large crystal represents section through center of crystal, perpendicular to the *b*-axis, showing four sectors. The {100} sectors contain {110} subsectors (*cf* text for explanation). Section corresponds to Figures 2A and 3B. Small crystal is also perpendicular to the *b*-axis, but section does not pass through center of crystal, showing two {11$\bar{1}$} and two {110} sectors. Section corresponds to Figures 2D and 3C. Specimen form McMurdo, Antarctica. C. Section about 40° oblique to the *b*-axis, showing only one {11$\bar{1}$} sector. Section corresponds to Figure 2E. Specimen from Goldfield, Nevada.

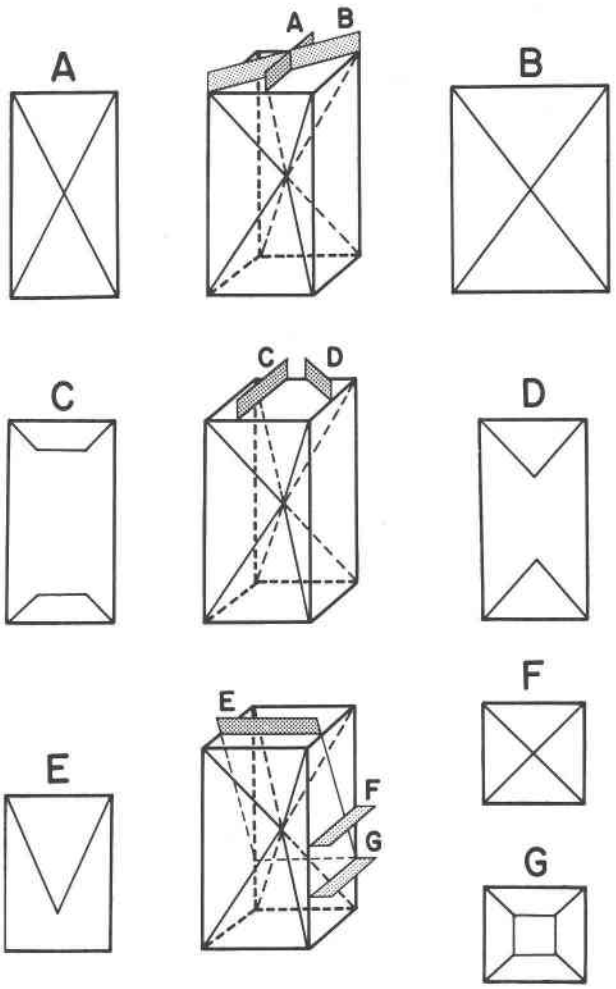

FIG. 2. Diagrammatic representation showing geometric relation between growth sectors according to the nature of their cross-sections relative to the idealized morphological model.

presence of three discrete domains whose maximum disorientation about the *b*-axis is about 2°. The disorientation is random, with neither the *a**- nor *c**-axis in common. Spots of approximately equal intensities can be related to the (100) and (11$\bar{1}$) sectors; therefore the weakest set of reflections may be attributed to a (110) subsector. In other words, the (100) and (110) are subsectors of a composite sector (*cf* Fig. 3B).

Unit cell dimensions derived from precession photographs of the {100} and {11$\bar{1}$} sectors from 3 crystals are shown in Table 1. The two sectors of crystal 1 were also examined on a single-crystal diffractometer, and least-squares refinements were performed using 12 centered reflections for each sector. The relatively large standard deviations for the data are probably due to chemical zoning and the

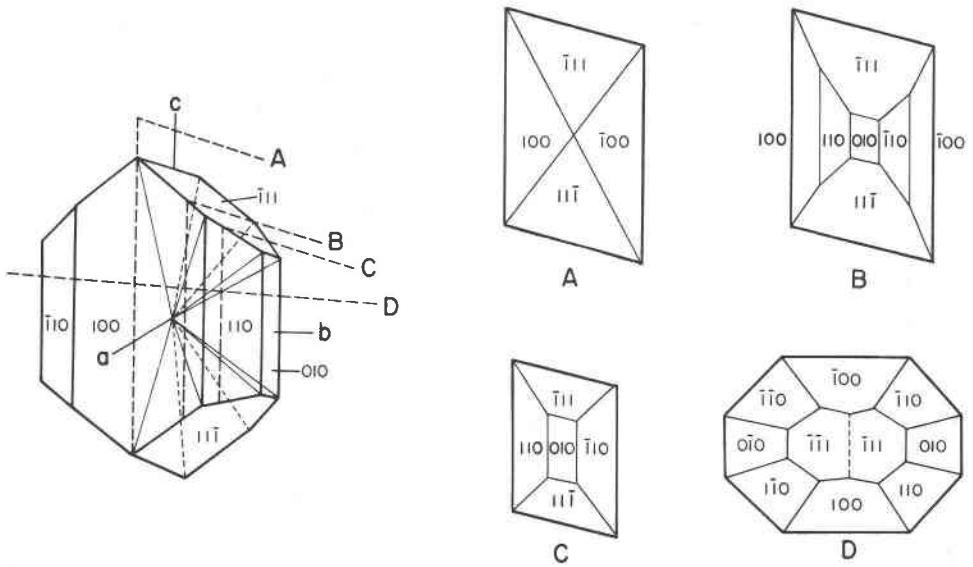

FIG. 3. A 12-pyramid morphological model of titanaugite showing how composite sectors can be derived.

small size of the crystal fragments (about 0.05 × 0.03 × 0.02 mm^3). Sector (11$\bar{1}$) of crystal 1 is extremely small; hence results obtained by the precession method are more reliable. In all three crystals, the parameter a of the {100} sector exceeds that for the {11$\bar{1}$} sector by about 0.02 Å, and c of the {100} is also longer by 0.02–0.03 Å. However, the b dimension of the {100} sector is considerably shorter, by 0.01–0.05 Å. Variations in the monoclinic angle β is small, less than 10 minutes of a degree.

Chemical

At least two crystals from each specimen containing well-defined sectors were chosen for chemical analyses by Mrs. J. F. Bower using a MAC electron probe at the Smithsonian Astrophysical Observatory. Four analyses were obtained from each sector from core to rim. Initial probe data were reduced to chemical analyses using a computer program written by Dr. J. A. Wood which corrects for background, deadtime drift, absorption, fluorescence, and atomic number.

TABLE 1. Unit Cell Dimensions of Titanaugites

Crystal	Locality	Sector	a (Å)	b (Å)	c (Å)	β
			PRECESSION			
1	Goldfield	(100)	9.761	8.854	5.280	106.20°
		(11$\bar{1}$)	9.744	8.906	5.259	106.15
2	Goldfield	(100)	9.762	8.892	5.287	106.17
		(11$\bar{1}$)	9.741	8.901	5.264	106.08
3	McMurdo	(100)	9.763	8.878	5.307	106.08
		(11$\bar{1}$)	9.743	8.907	5.266	105.95
Estimated Standard Deviation			0.01	0.01	0.005	0.08
			SINGLE-CRYSTAL DIFFRACTOMETER			
1	Goldfield	(100)	9.756(7)	8.851(7)	5.290(4)	106.20(4)
		(11$\bar{1}$)	9.762(9)	8.915(8)	5.259(6)	106.11(6)

Microprobe analyses show that two aspects of chemical zoning can be distinguished: zoning in the core-to-rim direction, and zoning in sectors. A decrease from core to rim of up to 5 percent Al (all figures in weight percent oxide) and a concomitant increase in the same direction of up to 5 percent Si are commonly observed, but these percentages may sometimes be as high as 8 percent, as in a specimen from Löbauerberg, Germany. The enrichment of Fe and depletion of Mg (about 1–2 percent) from core to rim suggests a normal trend of crystallization. A few crystals, however, showed a slight increase in Mg toward the rim accompanied by a sharp decrease in Al. There is generally a 0.5–1.0 percent decrease in the concentration of Ti from core to rim, but a few crystals showed little or no variation, and a few others even showed a slight increase in the same direction. The distribution pattern of Ca is almost constant from core to rim.

The other aspect of chemical zoning occurs in sectors. The prism sectors, {100}, {110}, and {010}, are enriched in Al, Ti, and Fe while the {11$\bar{1}$} sectors are enriched in Si and Mg, but no obvious sectoral preference of Ca was observed. Minor elements have not been analyzed. The pattern of elemental fractionation is remarkably consistent in all the specimens studied. Table 2 shows the average compositions (average of four analyses obtained from

TABLE 2. Average Composition of Sector-Zoned Titanaugites (Wt Percent)

Specimen Locality	MgO		Al_2O_3		SiO_2		CaO		TiO_2		FeO	
	(11$\bar{1}$)	(100)	(11$\bar{1}$)	(100)	(11$\bar{1}$)	(100)	(11$\bar{1}$)	(100)	(11$\bar{1}$)	(100)	(11$\bar{1}$)	(100)
Goldfield	17.49	14.20	3.10	7.15	50.36	45.93	19.82	20.62	0.82	1.95	8.54	9.91
McMurdo	14.70	10.89	4.41	10.65	49.98	42.42	21.85	21.89	2.11	4.83	6.82	8.24
Oka	11.05	9.40	9.57	12.71	41.79	39.28	24.68	24.40	3.33	4.76	7.42	8.60
Löbauerberg	11.35	10.05	4.00	6.96	48.65	45.89	24.12	23.49	2.37	4.02	7.56	8.89
Crawfordjohn	11.13	10.16	6.71	8.96	48.19	46.00	23.06	23.07	2.56	3.74	8.06	8.08

core and rim within the same sector of the same crystal) of typical crystals from five specimens. Compositions of {110} sectors are quite similar to those of {100}, but the {010} sectors show a slight depletion in Al and Ti.

Morphological Interpretations

If the sectors are considered to be a number of pyramids fitted together with their apices converging at the center of the crystal, then a minimum of six pyramids or sectors are required to constitute the parallelepiped shown in Figure 2. Sections parallel to the long axis passing through the center (A and B) show four triangular sectors with their apices converging at a central point (type 2a described above). Sections parallel to the long axis some distance from the center (C and D) show only two trapezoidal or triangular opposing sectors (type 2b). It is easy to see that any oblique section (E) cutting only four sectors (missing one prism and one basal sector) will show only one triangular sector (type 3). A section passing through the center parallel to the short axes (F) shows four triangular sectors, while sections also parallel to the short axes but some distance from the center (G) will show a core and four trapezoidal sectors (type 1).

Composite Sectors

If a crystal grew by adding successive layers of material parallel to the existing crystal faces, then the fully-grown crystal will be composed of as many growth pyramids as the number of crystal faces. All the "sectors" mentioned above were described by the index of growth layers parallel to the base of the growth pyramid. In thin sections, inner growth layers located near the apex of a sector may show an angle of tilt different from that of the outer layers when rotated to vertical on the universal-stage, and in cases where accurate measurements are possible, the inner and outer growth layers can be identified as distinct co-zonal planes. Such sectors are composite in nature, *i.e.*, they contain parts of two or more growth pyramids. Figure 3 shows how composite sectors can be derived. It is not uncommon to have three subsectors within one composite sector, but the inner-most subsector at the center of the crystal is usually too small for optical measurements. Flexures at sector boundaries mark the junctions of subsectors. The presence of one or two flexures on the boundary of a triangular sector implies the presence of two or three subsectors, respectively.

Each sector or growth pyramid has a crystal face as its base, hence the pyramid has as many sides as the number of edges of the crystal face. When a section is cut close to one of these edges on the base of a growth pyramid, the outermost layers of that pyramid or sector are represented by nothing more than a slender "rim." This "rim," generally very well-defined and clear, may taper off some distance down the edge, or may occur on two adjacent or two opposite sides of the crystal, depending on the obliquity of the section with respect to the sectors. Such a "rim" does not surround the whole crystal as in the case of a reaction rim.

The presence of subsectors has also been confirmed by the tripling of X-ray spots of a crystal fragment containing a (100) and a (11$\bar{1}$) sector. The third spot can be attributed to a small portion of a (110) sector occurring adjacent to the (100). The optical indicatrix axes of the (100) and (11$\bar{1}$) sectors of this crystal showed a maximum disorientation of about 10°, but only a 2° rotation was observed on an X-ray precession photograph of the same crystal. The discrepancy between the amount of disorientation can be explained by rotations of the optical indicatrices due to changing chemical compositions between sectors as evidenced by changes in extinction angles, $Z \wedge c$; and the 2° rotation detected by X-rays can be accounted for by a misfit displacement between adjacent sectors which have appreciable differences in chemistry and cell dimensions. Because of the differences in chemical composition, considerable strain exists between adjacent sectors. During or subsequent to quenching or crystallization, strain release was achieved by

dislocation climbs whereby fault surfaces were formed at the boundary of growth sectors. Arem (1970) observed in idocrase crystals large differences in extinction positions between sectors, but the crystals gave essentially single crystal X-ray diffraction patterns (personal communication). This may also be a chemical effect.

Discussions of Growth

Mechanisms

The origin of hourglass structures is no doubt related to the differential rate of growth and the preferential uptake of elements with respect to crystallographic directions. Hourglass patterns or the Maltese cross in the case of cubic crystals are common in crystals grown in solutions containing a low concentration of a color dye. Molecules of the dye appear as adsorbed impurities in non-adjacent sectors (Buckley, 1951; Slavnova, 1959). In the case of pyroxenes, the elements Al and Ti, which substitute for Si and Mg, may also be considered impurities, except that they are soluble instead of adsorbed, or substitutional instead of interstitial. To understand this phenomenon, it is necessary to analyze a large number of interdependent factors at a growing crystal face: rate of growth, structure of growing layers, and availability of ions in the melt. Some of these factors are also related to the problem of heat and mass transfer or diffusion.

Donnay and Harker (1937) pointed out the importance of space group symmetry in predicting the morphological importance of crystal faces. Their basic principle, that of Bravais, states that the dominant forms have higher reticular density (number of atoms per unit area) or large interplanar spacing. Their method was purely geometrical and took no consideration of ionic interactions within the crystal or of the external environment in which the crystal grew. Hartman and Perdok (1955; Hartman, 1963, 1967) tried to relate morphology to structure which they pictured as composed of periodic bond chains. They classified crystal faces into three types: flat, stepped, and kinked, respectively having two, one, or none of the strong chains parallel to them. Flat faces, having the highest reticular density, are the slowest-growing, as the growth mechanism is equivalent to a two dimensional nucleation, while kinked faces grow the fastest, as atoms can be attached with ease in holes on the crystal surface. Because of their fast growing rate, kinked faces will ultimately outgrow themselves and disappear. Stepped faces belong to an intermediate type. Hartman and Perdok took into account only attachment energies of atoms and interaction energy in the first coordination sphere. However, this is not sufficient for explaining rapid growth at high supercooling or when polymerization had occurred even in the liquid phase, such as in the case of a silicate melt (Hess, 1971). In studies of crystal growth, as a result, the external medium cannot be ignored.

Rate of Growth

An outstanding feature in sector-zoned crystals is the pronounced layering parallel to the base of the growth pyramids. The periodic nature of growth layers, especially common in melt-grown metal crystals, has been correlated to thermal or constitutional supercooling in the melt, which creates a form of convective instability called overstability in which a synchronous coupling of the conducted and convected heat flows takes place (Chandrasekhar, 1961; Hurle, 1967). In order that a crystal may grow, supercooling of the melt is necessary, and the rate of growth depends on the degree of supercooling. As elements in the dispersed phase are incorporated in the solid, the heat of fusion accumulated at the solid-liquid interface gives rise to convections. Cyclic convections of this type may be related to the origin of regular periodic growth layers observed in this study. The thickness of these macroscopic growth layers is controlled by the frequency of these convective cycles. The rate of growth is thus dependent on how fast heat is dissipated from the growing crystal face.

A morphological study of the crystals used in this study also revealed that sector boundaries are planar surfaces, except at the flexures which mark the junctions of subsectors. Sector boundaries are able to retain their direction only if all faces of the crystal grew at constant relative velocities. When a grain has a certain length-to-width ratio, for instance, the geometry outlined by the growth layers indicates that this ratio has been constant at all stages of growth, or that the morphology has been stable. To maintain the habit or shape stability, different types of faces must grow at constant relative velocities. The $\{11\bar{1}\}$ faces in the hourglass-structured pyroxenes are faster-growing than the $\{100\}$, $\{110\}$, and the $\{010\}$, as can be seen from the relative thicknesses of the growth layers (*e.g.*, Fig. 1B). Faces of the form $\{001\}$ are absent. As $\{001\}$ is the fastest-

growing direction because of its disposition relative to the SiO_3 chains, it is not expected to be present in fast-growing pyroxenes. Had there been a lesser degree of supercooling at the time of crystallization, the rate of deposition on {001} would have been more compatible to that on the prism faces, and the appearance of {001} would have become more likely.

Structure of Growing Layers

On the (100) face of clinopyroxenes, two types of SiO_3 chains parallel to the *c*-axis are exposed. They are alternating chains with the apices of the silicate tetrahedra pointing along $+a^*$ and $-a^*$. The apical oxygen atoms on a growing layer are probably responsible for capturing cations from the melt. Each apical oxygen is bonded to two *M*1 and one *M*2 ions. In a typical clinopyroxene structure such as that of diopside, the octahedral *M*1 sites are usually occupied by Mg, while the larger *M*2 sites, coordinated by eight oxygen atoms, are occupied by Ca. It is also possible to substitute other metal ions such as Fe^{2+}, Fe^{3+}, or Ti^{4+} in the *M*1, and Fe^{2+} in the *M*2 sites. The (100) face, having the highest reticular density, is "flat", or parallel to repeating planes of cations and layers of linked SiO_3 chains (vertically oriented in Figure 4A).

The SiO_3 chains on the (010) face are paired with their apical oxygens face to face. The *M*1 sites lie between apices of the silicate tetrahedra, while the *M*2 sites lie between their bases. Parallel to (010) are regular double layers of *M*1 sites alternating with double layers of *M*2 sites (Fig. 4A). In the process of growth, double layers of *M*1 sites may be filled immediately after depositions of SiO_3 chains because of attractions of the apical oxygens. This is followed by the formation of double *M*2 layers which tie the chains together.

The pyroxene structure also shows that parallel to the (110) face, there are double layers of *M*1 and *M*2 sites akin to those of the (010) face described above, except that the double *M*1 layers are more closely spaced than the double *M*2 layers which give rise to the (110) cleavage between the *M*2 layers (Fig. 4B). The cation sites are also aligned in planes parallel to (11$\bar{1}$), but with single layers of *M*2 sites alternating with double layers of *M*1 sites (Fig. 5).

In contrast to the other faces so far considered, the (001) face at any level in the c^* direction contains an equal number of *M*1 and *M*2 sites. The (001) face is a plane at which the SiO_3 chains terminate,

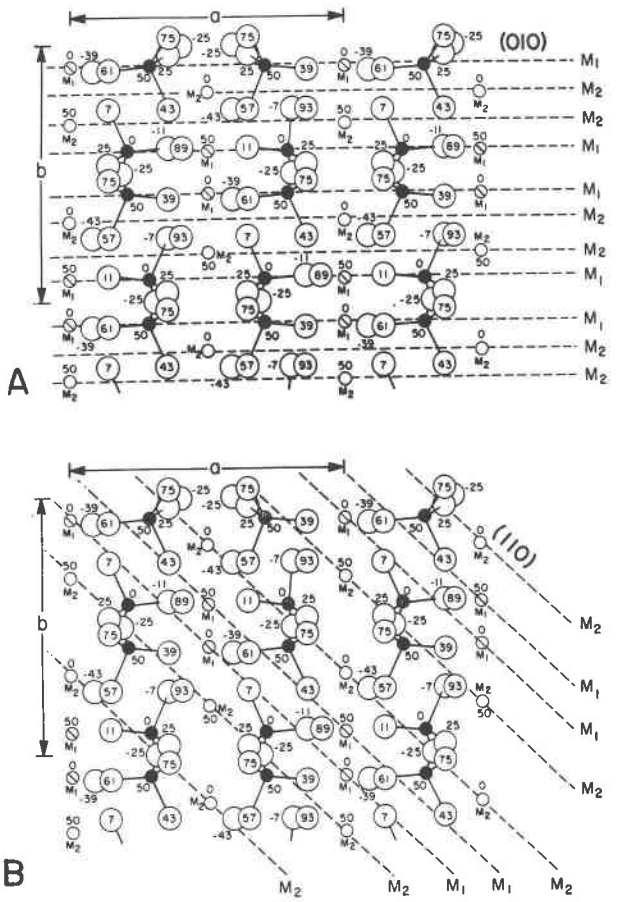

FIG. 4. Atomic structure of clinopyroxene as viewed along *c* (modified from Deer *et al*, 1963). A. (100) planes (vertical) parallel to layers containing both *M*1 and *M*2 sites, and layers of linked SiO_3 chains. (010) planes (horizontal) parallel to alternating double *M*1 and *M*2 layers. B. (110) planes parallel to alternating double *M*1 and *M*2 layers.

and in between the chains, large holes are present. Every hole or *M* site is surrounded by four silicate tetrahedra, each of which belongs to a different chain. The probability that an ion enters the *M*1 or the *M*2 site is the same. The SiO_3 chains can be lengthened by adding silicate tetrahedra which probably already exist as (SiO_4^{4-}) in the melt.

To summarize, the structural distribution of *M* sites in clinopyroxenes shows that the prism faces (110) and (010) are parallel to double layers of *M*1 and *M*2 sites. The *M*1 sites, located between apices of SiO_3 chains, are probably filled as the chains are deposited. This means that when layers of material crystallize on these faces, a large number of Mg ions, for example, would be required to fill two layers of *M*1 sites, followed by depositions of Ca ions which fill

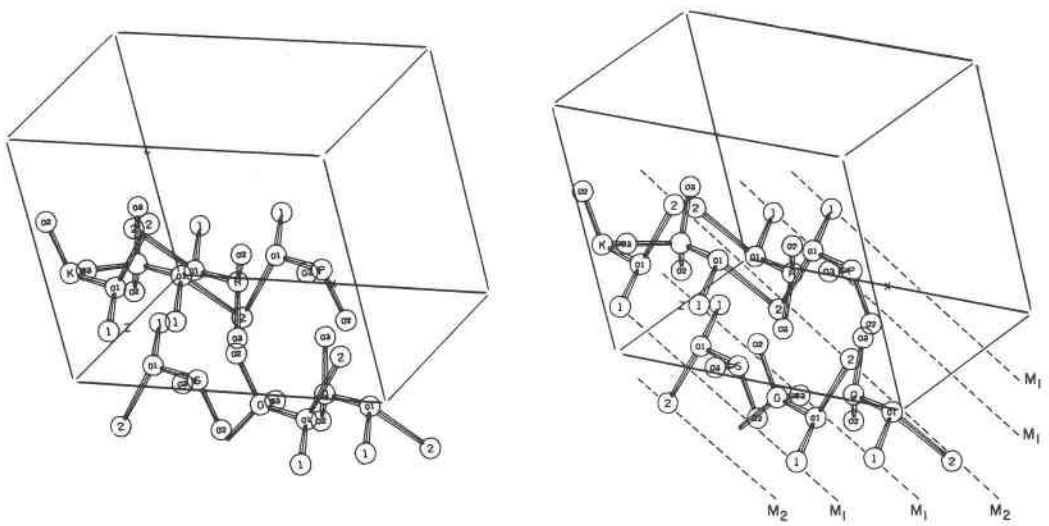

FIG. 5. Stereoscopic view parallel to (11$\bar{1}$) plane of titanaugite showing alternating double $M1$ and single $M2$ layers. Only units of ($M1$ $M2$ SiO_3) are drawn. $M1$ and $M2$ sites are labelled 1 and 2, respectively. Oxygen atoms are labelled O1, O2, O3, silicon atoms are designated by letters G, K, P, Q, R, S, and one silicon atom has no label. Figure plotted by Professor Jesse Schilling, Trinity University, San Antonio, Texas, using computer program ORTEP, and coordinates of a titaniferous Al-pyroxene (Peacor, 1967).

the succeeding double layers of $M2$ sites. The (100) face is developed by depositions of a large number of cations of both types, followed by depositions of silicate chains. The (11$\bar{1}$) face is parallel to single $M2$ layers alternating with double $M1$ layers. Development of the (11$\bar{1}$) face is achieved by the concomitant addition of cations and silicate tetrahedra. Thus, the prism faces can be interpreted as slow-growing due to the time required to accumulate large quantities of $M1$ and $M2$ ions when double layers of M sites are filled on the (010) and (110) faces, and to form complete layers of M sites on the (100) face. The (001) is a kinked face on which material can be attached by lengthening the SiO_3 chains and filling the cation sites simultaneously. In a melt of low viscosities where there is free migration of the elements, the (001) face grows so fast that it may eliminate itself, and in its place the slower-growing (11$\bar{1}$) face is found.

Diffusion Model

Under hydrostatic pressures, the condition for equilibrium in a melt is that the chemical potential of the liquid equals the chemical potential of the solid. In liquids surrounding rapidly growing crystals, disequilibrium exists. At the solid-liquid interface, the liquid adjacent to the growing crystal face is enriched in components not utilized by the crystallizing phase. This liquid is described as constitutionally supercooled (Knight, 1967). In Figure 6, it is assumed that the crystal grew as fill-in dendrites. In quenching experiments of basaltic melts by the writer (and by D. W. Chipman, personal communication), the first crystallizing phase which appeared in the melt was in the form of dendrites. Dendritic growth seems most common in the early stages of crystal growth (Buckley, 1951), and in extrusive lava flows such as in the McMurdo basalts. In the fast-growing direction of pyroxene crystals, the melt may be rapidly depleted in Mg and Si, but not in the melt adjacent to the slower-growing faces. This difference in concentration or the chemical gradient, G_1, allows diffusion to take place (Fig. 6). On the other hand, the melt in the fast-growing direction is constitutionally supercooled with respect to elements such as Al, Ti, and Fe, thus the chemical gradient, G_2, allows diffusion in the opposite direction. Once generated, the diffusion cycle will perpetuate itself with continued growth.

This model can be used to interpret the pattern of chemical substitutions in sector-zoned pyroxenes with or without evoking the fill-in dendrite growth mechanism. A dendritic model is drawn in Figure 6 because many dendritic crystals have been observed in several basaltic rocks as well as in experimentally quenched basaltic melts. In a situation when only one type of atom, or only silicate chains, may be incorporated

into the growing layer of a crystal, a large quantity of that substance is required. If the required substance is not readily available, substitutions may become necessary. On the (11$\bar{1}$) face of clinopyroxenes, the silicate chains can be extended by the addition of silicate tetrahedra while Mg or Ca simultaneously occupy the *M*1 or *M*2 sites. Thus, neither Mg, Ca, nor silicate tetrahedra are depleted so rapidly that substitutions by other elements become necessary; therefore, the (11$\bar{1}$) face is relatively free of impurities, or, in other words, relatively enriched in Mg and Si which are most suitable for the normal clinopyroxene structure. But, because of its comparatively rapid rate of growth, the liquid adjacent to the (11$\bar{1}$) face becomes supercooled with respect to impurity elements (such as Fe, Ti, and Al) left in the melt.

During the growth of a (100) face, large amounts of Ca and Mg ions are required to fill layers composed entirely of *M*1 and *M*2 sites. At this time, the melt is rapidly depleted in these elements, so that other elements such as Ti, which normally does not enter the pyroxene structure, may be incorporated. Depositions of the succeeding layers of silicate chains deplete Si in the melt in the immediate vicinity of the crystal face, enabling Al to substitute for Si, particularly in an undersaturated liquid. The alternating layers of cations and silicate chains on the (100) face were also noticed by Nakamura (1973) who emphasizes, rather, the importance of the size, shape, and coordination of partially formed structural sites on a growing crystal surface in his interpretation of sector zoning of igneous clinopyroxenes. He reported Ca deficiency in the {100} sectors relative to the {110} and {010} of crystals developed in a magma supersaturated with Ca-poor pyroxene. This may be explained by the rapid depletion of Ca during depositions of the cation layers on the {100} face, so that 40 percent of the *M*2 sites become occupied by Mg, Fe, Ti, and Mn.

The (010) and (110) faces grow by filling double layers of *M*1 and *M*2 sites in succession, and if a large quantity of Mg atoms are not readily available, Fe and Ti may enter some of the *M*1 sites. The *M*2 sites seem to be almost completely occupied by Ca in all types of sectors, as has also been confirmed by chemical and Mössbauer studies. An explanation for this is that most of the rocks used in this study have a superabundance of Ca. As the chains are deposited on the (010) and (110) faces, the apical oxygens capture the *M*1 ions. Thus large amounts of Si and Mg will be used up at this time, allowing Al to substitute for Si, Fe and Ti for Mg.

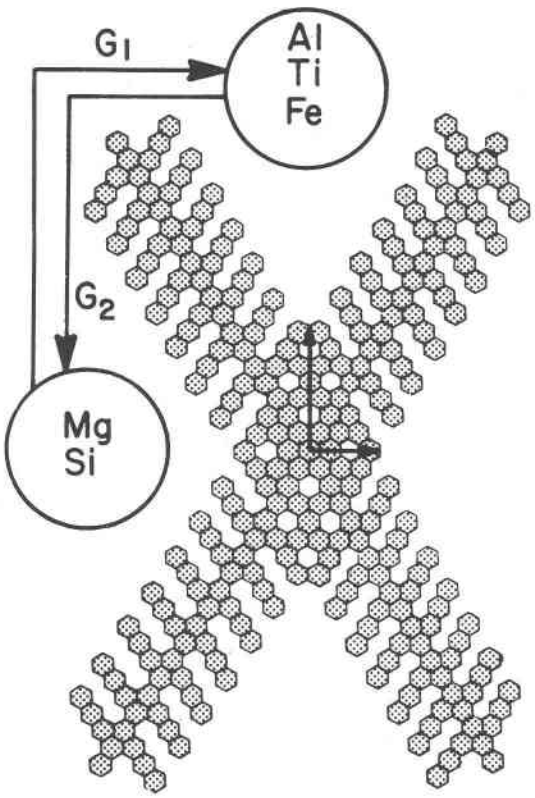

FIG. 6. Crystal growth as fill-in dendrites. Velocities of growth are proportional to lengths of arrows on crystal. Constitutional supercooling of elements inside circle adjacent to crystal face is caused by different velocities of growth. G_1 and G_2 are chemical gradients which allow diffusion to take place.

Because more Fe, Ti, and Al are incorporated into the prism sectors than into the {11$\bar{1}$} sectors, these elements are depleted in the liquid adjacent to the prism faces. Because of the slower rate of growth of the prism sectors as well as the reason given above, the liquid adjacent to the prism faces has a higher concentration of Mg and Si than in the liquid adjacent to the {11$\bar{1}$} sectors. In short, different types of chemical substitutions occurring in different sectors can be explained by the structures of the growing layers and their mechanisms of growth, while the supply and availability of substituting elements are accounted for by chemical gradients created by the faster rate of growth of the {11$\bar{1}$} sectors and the slower rate of growth of the prism sectors.

Cohen (1960) found that Al is preferentially incorporated into the prism sectors of quartz, while the

rhombohedral sectors are free from substitutional Al. He attempted to explain this phenomenon by referring to the voids in the quartz structure parallel to the *c*-axis as channels facilitating free exchange of impurities with the solution during growth. The validity of this argument may be questioned as impurities may also be able to enter the crystal structure through these voids. As shown below, the application of the diffusion mechanism seems appropriate. Since [0001] is the fastest-growing direction in quartz (hence {0001} is extremely rare), the crystallizing medium in that direction is rapidly depleted in Si and supercooled with respect to impurities such as Al. These impurities will diffuse toward the slower-growing prism faces and become incorporated.

Sectoral Growth in Lunar Pyroxenes

One of the most spectacular and interesting features found in the Apollo 11 igneous rocks is the hourglass structure in clinopyroxenes. This feature occurs abundantly in sample 10047,42, and two of the crystals studied by Carter *et al* (1970) are shown in Figure 7. Both crystals were cut parallel to the *c*-axis. The view of crystal A is nearly in the direction of the *b*-axis, and crystal B is cut above 40° oblique to *b*. In both cases, no growth layering can be observed, therefore growth sectors were identified only with the aid of the {110} cleavages and the assumption that the 12-pyramid morphological model (Fig. 3) does apply. In agreement with observations on terrestrial augites, the light brown sectors are {110}, and possibly also {010}, located at the core (Fig. 3C). The colorless sectors are the $\{11\bar{1}\}$, although other possibilities such as the {011}, $\{\bar{1}01\}$, or {001} cannot be eliminated. The colorless sectors are relatively enriched in Mg and Si, and the light brown prism sectors are relatively enriched in Ca, Ti, and Al.

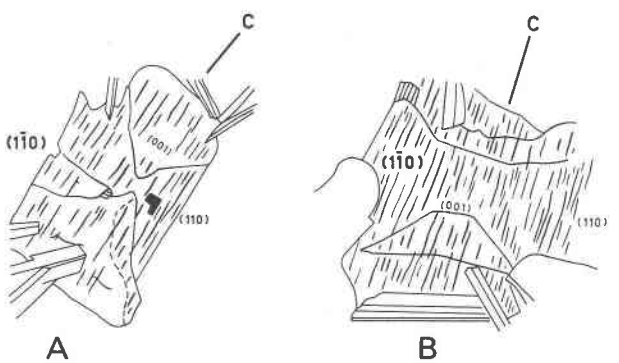

FIG. 7. Sector-zoned augite crystals from Apollo 11 sample 10047, 42.

Similar to terrestrial titanaugites, the diffusion mechanisms caused by the differential rates of growth and degrees of supercooling around the growing crystal might have been responsible for the observed sectoral chemical fractionation. This principle also satisfactorily explains the growth of a martini-glass clinopyroxene in a vug from Apollo 11 rock 10050 reported by Bence and Papike (1971). The crystal has a funnel-shaped pigeonite core, with subcalcic augite sheathing around the stem. The reported tabular pigeonite nucleus probably grew fastest in the *c* direction, depleting the melt or vapor in that direction of the pigeonite components, but, at the same time, the same vicinity was constitutionally enriched in the augite components. This enabled migration of the augite components to the prism faces and pigeonite components to the reported {011} faces. Thus, pigeonite and augite were able to grow concomitantly, but in distinctly different sectors of the crystal. In their analysis, Bence and Papike reported a continuous change in composition from a pigeonite core to a composition approaching that of the sheathing subcalcic augite in the [001] direction. This trend seems to be related to a decrease in temperature which may or may not be accompanied by a change in composition of the surrounding melt or vapor. Also, at a lower temperature, the crystallizing medium becomes more viscous, resulting in a decreased rate of diffusion. This is coupled with a decreased rate of growth which, in turn, makes constitutional supercooling less marked and diffusion gradients less steep. At this stage, sectoral fractionation is no longer expected to take place. Takeda (1971) also found a crystal in a vug from Apollo 12 rock 12052. He reported a honey-yellow core of pigeonite overgrown by a dark brown augite. Boundaries between the two phases are sharp. He believed (personal communication) that as the pigeonite core grew, the surrounding medium was supercooled with respect to augite components, and, with a drop in temperature, augite was immediately deposited epitaxially on the pigeonite core. In this respect, the diffusion model not only explains sectoral growth, but may also be modified to solve other problems in genetic mineralogy.

Summary and Conclusions

Titanaugites in basaltic rocks commonly display a 12-pyramid morphology (Fig. 3), and the constituent sectors are layer-structured. Each of the 4 kinds of growth faces, {100}, {110}, {010}, and $\{11\bar{1}\}$, grew by a particular mechanism of its own.

The rate of growth is structurally controlled, but is also sensitive to external conditions such as the degree of supercooling and rate of diffusion. Sector zoning in composition is strongly reflected by the optical properties and unit cell dimensions. However, no simple relationships can be found between changes in unit cell dimensions with variations in individual substitutions, since substitutions in clinopyroxenes are often multiple in character. Variations in unit cell dimensions and chemical compositions between sectors are quite significant, and this fact should be considered in X-ray powder diffraction work or wet chemical analyses when sectors cannot be separated out. A model showing constitutional supercooling and diffusion mechanisms as responsible for sectoral growth is proposed.

Similarities among terrestrial and lunar clinopyroxenes studied include pronounced sector zoning detected optically and chemically, but there are also dissimilarities such as the presence of pigeonite intergrowths and complexities in chemistry in the lunar pyroxenes which are absent in the terrestrial titanaugites. From this study, it is concluded that sectoral chemical fractionation observed in lunar clinopyroxenes indicates rapid disequilibrium growth at high temperature. The lack of microscopic growth bands suggests that the crystals grew in a melt of low viscosities and high diffusion rates, so that the heat of fusion produced during crystallization was dissipated continuously rather than accumulating at the solid-liquid interface to set up convection cycles such as were probably responsible for the origin of growth bands observed in terrestrial titanaugites.

The terrestrial rocks in which sector-zoned augite crystals occur are alkali-rich, and of a continental origin. Verhoogen (1962) showed on thermodynamic grounds that high temperature favors the entry of Ti into pyroxenes, and that substitutions of Al for Si can occur only at high temperatures. As the solubility of Ti increases with the amount of Al that can be substituted for Si in the tetrahedral sites of pyroxenes, more Ti is expected in pyroxenes in undersaturated magmas having a low silica activity. Yagi and Onuma (1967) demonstrated experimentally that at high pressures (10–25 kbar), the solubility of Ti in diopside decreases nearly to nil. All these point to the conclusion that sector-zoned titanaugites are quenched products originated from a rapid, disequilibrium crystallization at high temperature and relatively low pressure. If alkaline olivine basalts are believed to have originated at greater depth than tholeiitic basalts, then titanaugite crystals in the former must have formed quite near the earth's surface at shallow depths or even during extrusion.

Acknowledgments

Mrs. J. F. Bower kindly performed the microprobe analyses, Messrs. Y. S. Cheung and H. K. Kwan of the University of Hong Kong helped prepare some of the illustrations, Professor J. Schilling plotted Figure 5, and Professor N. L. Carter read and criticized the first draft of the manuscript. This work was supported by NASA and NSF grants to Professor N. L. Carter at Yale University, and a Faculty Research Award at the City University of New York.

References

AREM, JOEL (1970) *Crystal Chemistry and Structure of Idocrase*. Ph.D. dissertation, Harvard University.

BARTON, PAUL B., JR., PHILIP M. BETHKE, AND PRIESTLY TOULMIN, 3RD (1963) Equilibrium in ore deposits. *Mineral. Soc. Am. Spec. Pap.* **1**, 171–185.

BENCE, A. E., AND J. J. PAPIKE (1971) A martini-glass clinopyroxene from the moon. *Earth Planet. Sci. Lett.* **10**, 245–251.

BUCKLEY, H. E. (1951) *Crystal Growth*. Wiley, New York.

CARTER, N. L., I. S. LEUNG, H. G. AVE'LALLEMANT, AND L. A. FERNANDEZ (1970) Growth and deformation structures in silicates from Mare Tranquilitatis. *Proc. Apollo 11 Sci. Conf.* **1**, 267–285.

CHANDRASEKHAR, S. (1961) *Hydrodynamic and Hydromagnetic Stability*. Clarendon Press, Oxford.

COHEN, A. J. (1960) Substitutional and interstitial aluminum impurity in quartz, structure and color center interrelationships. *J. Phys. Chem. Solids*, **13**, 321–325.

DEER, W. A., R. A. HOWIE, AND J. ZUSSMAN (1963) *Rock-forming Minerals*. Longmans, London.

DONNAY, J. D. H., AND DAVID HARKER (1937) A new law of crystal morphology extending the law of Bravais. *Am. Mineral.* **22**, 446–467.

FARQUHAR, OSWALD C. (1960) Occurrences and origin of the hourglass structure. *Rep. 21st Sess. Int. Geol. Congr., Norden*, **21**, 194–200.

FRONDEL, C., W. H. NEWHOUSE, AND R. F. JARRELL (1942) Spatial distribution of minor elements in single-crystals. *Am. Mineral.* **27**, 726–745.

GRAY, NORMAN H. (1971) A parabolic hourglass structure in titanaugite. *Am. Mineral.* **56**, 952–958.

HALFERDAHL, L. B. (1961) Chloritoid: its composition, X-ray and optical properties, stability, and occurrence. *J. Petrol.* **2**, 49–135.

HARTMAN, P. (1963) Structure, growth and morphology of crystals. *Z. Kristallogr.* **119**, 65–78.

——— (1967) The dependence of crystal morphology on crystal structure. *Growth of Crystals*, **7**, 3–18. N. N. Sheftal', Ed., translated from Russian, Consultant Bureau, Inc., New York.

———, AND W. G. PERDOK (1955) On the relations be-

tween structure and morphology of crystals, I, II, and III. *Acta Crystallogr.* **8,** 49–52, 521–524, 525–529.

HESS, PAUL C. (1971) Polymer model of silicate melts. *Geochim. Cosmochim. Acta,* **35,** 289–306.

HOLLISTER, LINCOLN S. (1970) Origin, mechanism, and consequences of compositional sector-zoning in staurolite. *Am. Mineral.* **55,** 742–766.

———, AND ALEXANDER J. GANCARZ (1971) Compositional sector-zoning in clinopyroxene from the Narce Area, Italy. *Am. Mineral.* **56,** 959–979.

HURLE, D. T. (1967) Thermo-hydrodynamic oscillations in liquid metals: the cause of impurity striations in melt-grown crystals. *Crystal Growth,* E. H. Steffen Peiser, *Proc. Int. Conf. Crystal Growth,* Boston, 1966.

KASTNER, MIRIAM (1970) An inclusion hourglass pattern in synthetic gypsum. *Am. Mineral.* **55,** 2128–2130.

KNIGHT, CHARLES A. (1967) *The Freezing of Supercooled Liquids.* D. Van Nostrand Co., Inc.

LEUNG, IRENE S. (1971) Sectoral growth in aluminous titanaugites (abstr.) *EOS Trans. Am. Geophys. Union* **52,** 382.

NAKAMURA, YASUO (1973) Origin of sector-zoning of igneous clinopyroxenes. *Am. Mineral.* **58,** 986–990.

PEACOR, DONALD R. (1967) Refinement of the crystal structure of a pyroxene of formula $M_1M_{11}(Si_{1.5}Al_{0.5})O_6$. *Am. Mineral.* **52,** 31–41.

PELIKAN, A. (1896) Ueber den Schichtenbau der Krystalle. *Mineral. Petrogr. Mitt.* **16,** 1–64.

PRESTON, J. (1966) An unusual hourglass structure in augite. *Am. Mineral.* **51,** 1227–1233.

SLAVNOVA, E. N. (1959) The main trends in the study of inorganic crystals containing organic impurities. *Growth of Crystals,* **2,** 166–174. A. V. SHUBNIKOV AND N. N. SHEFTAL', Eds., translated from Russian, Consultant Bureau, Inc., New York.

SMITH, A. L., AND I .S. E. CARMICHAEL (1969) Quaternary trachybasalts from southeastern California. *Am. Mineral.* **54,** 909–923.

STRONG, D. F. (1969) Formation of the hour-glass structure in augite. *Mineral. Mag.* **37,** 472–479.

TAKEDA, HIROSHI (1971) Euhedral clinopyroxenes in a vug from an Apollo 12 rock (abstr.). *EOS Trans. Am. Geophys. Union,* **52,** 271.

VANCE, JOSEPH A. (1965) Zoning in igneous plagioclase: patchy zoning. *J. Geol.* **73,** 636–651.

VERHOOGEN, JOHN (1962) Distribution of titanium between silicates and oxides in igneous rocks. *Am. J. Sci.* **260,** 211–220.

YAGI, KENZO, AND KOSUKE ONUMA (1967) The join $CaMgSi_2O_6$–$CaTiAl_2O_6$ and its bearing on the titanaugites. *J. Fac. Sci. Hokkaido Univ. Ser. 4,* **8,** 463–483.

Manuscript received, May 18, 1973; accepted for publication, September 27, 1973.